Spectral evolution of angularly resolved third-order harmonic generation by infrared femtosecond laser-pulse filamentation in air

Hui Xiong,[1] Han Xu,[1] Yuxi Fu,[1] Ya Cheng,[1,*] Zhizhan Xu,[1,†] and See Leang Chin[2]
[1]*State Key Laboratory of High Field Laser Physics, Shanghai Institute of Optics and Fine Mechanics, Chinese Academy of Sciences, P.O. Box 800-211, Shanghai 201800, China*
[2]*Centre d'Optique, Photonique et Laser (COPL) and Département de Physique, de Génie Physique et d'Optique, Université Laval, Québec, Québec, Canada G1K 7P4*
(Received 26 January 2008; revised manuscript received 3 March 2008; published 1 April 2008)

We experimentally investigate the evolution of an angularly resolved spectrum of third harmonic generated by infrared femtosecond laser pulse filamentation in air. We show that at low pump intensity, phase matching between the fundamental and third-harmonic waves dominates the nonlinear optical effect and induces a ring structure of the third-harmonic beam, whereas at high pump intensity, the dispersion properties of air begin to affect the angular spectrum, leading to the formation of a nonlinear X wave at third harmonic.

DOI: 10.1103/PhysRevA.77.043802 PACS number(s): 42.65.Tg, 42.65.Jx

I. INTRODUCTION

Femtosecond filamentation has drawn broad attention due to its potential application in remote sensing [1–3], lightning control [4–6], pulse compression [7,8], supercontinuum generation [9,10], and so on. Intensive studies have been undertaken to fully understand the nonlinear optical phenomena occurring during filamentation [11–13]. In a simple physical picture, the filamentation process is a result of dynamic balance between self-focusing due to Kerr nonlinearity and defocusing due to linear diffraction and plasma. The peak intensity inside the filament generated in air can be as high as 5×10^{13} W/cm^2, which is sufficient for generating third-harmonic (TH) radiation [14–17]. In addition to air, TH generation through filamentation has also been observed in atomic and molecular gases [16,18–21], as well as liquids [22]. Conversion efficiency in air up to 0.2% has been observed [23]. The high conversion efficiency can be interpreted either by phase locking between the generated TH and the fundamental inside the filament, which maintains the phase-matching condition for third-harmonic generation (THG) over a long distance [17], or by a three-wave mixing (ETWM) picture [24,25].

Recently, we reported the formation of an X-shaped TH wave by ultrashort infrared (IR, 1270 nm wavelength) pulse filamentation in air [26]. This was achieved by recording angularly resolved spectra of the TH waves centered at ~420 nm wavelength. The angular resolved spectrum [27], which is also called the far-field or K-Ω spectrum, has been proven to be a powerful tool in the investigation of ultrashort pulse propagation [25,28]. In this paper, we attempt to gain deeper insight into the physical processes responsible for the generation of a TH X wave by studying the evolution of the angular spectrum of the TH. We will show that at low pump intensity, phase matching between the fundamental and third-harmonic waves dominates the nonlinear optical effect and induces a ring structure of the third-harmonic beam, whereas at high pump intensity, the dispersion properties of air govern the angular spectrum, leading to the formation of a TH X wave.

II. EXPERIMENTAL

The experimental setup is shown in Fig. 1. The tunable IR laser pulses are generated by an optical parametric amplifier (OPA, TOPAS-C, Light Conversion, Inc.) pumped by a commercial Ti:sapphire laser system (Legend, Coherent, Inc.). The Ti:sapphire laser, operated at a repetition rate of 1 kHz, provides 40 fs (FWHM) laser pulses with a central wavelength at 795 nm and a single pulse energy of 2.5 mJ. The central wavelength of the signal pulse generated by OPA is fixed at 1270 nm throughout this experiment, and the spectral width (FWHM) is approximately 65 nm, as shown in the inset of Fig. 1. By using a pair of dielectric coated broadband mirrors ($R1$, $R2$, high reflection within 1100–1300 nm), the idler pulse centered at ~2100 nm is suppressed. After that, the signal pulse is focused into air using a gold-coated concave mirror (GM) with a focal length of 25 cm to generate a

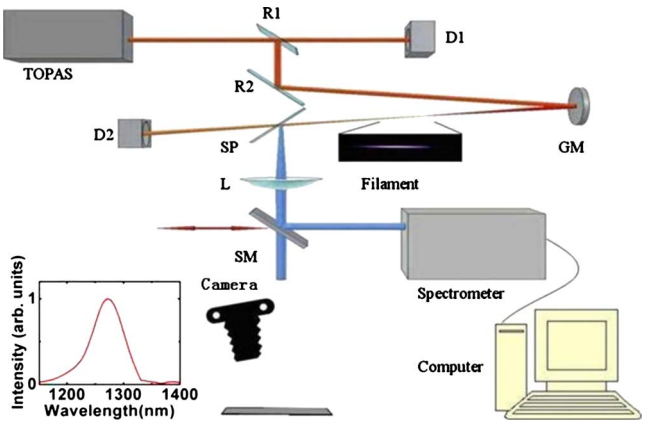

FIG. 1. (Color online) Schematic of experimental setup. $R1$,$R2$: dichroic mirrors high-reflectively coated at 1100–1300 nm. $D1$, $D2$: beam dampers. GM: gold-coated concave mirror. SP: dichroic beam splitter, L: lens. SM: silver-coated mirror.

*ycheng-45277@hotmail.com
†zzxu@mail.shcnc.ac.cn

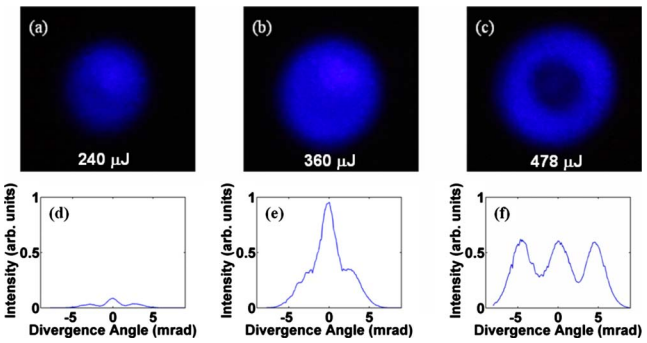

FIG. 2. (Color online) Digital camera captured spatial beam patterns of TH beams (a)–(c) and the corresponding intensity profiles (d)–(f). Pump energies are 240 μJ in (a) and (d), 360 μJ in (b) and (e), and 478 μJ in (e) and (f).

single light filament. A dichroic beam splitter (SP), which is high-reflectively coated at ~400 nm is used to separate the TH wave from the fundamental IR wave.

Angular resolved spectra of TH waves are recorded by an angular resolved spectrometer, which consists of a positive lens L with a focal length of 30 cm and an imaging grating spectrometer (SpectraPro 300i, Acton). The lens is used to collimate the TH emission, and a silver-coated mirror (SM) further redirects the TH beam into the imaging spectrometer. Far-field spatial patterns of the TH waves are captured with a digital camera (D50, Nikon) by removing the lens L and the silver-coated mirror SM.

III. RESULTS AND DISCUSSIONS

In Figs. 2(a)–2(c), we show the spatial beam patterns of TH beams captured by the digital camera at different pump energies, and the corresponding intensity profiles are presented in Figs. 2(d)–2(f). Here, the intensity profiles are obtained by integrating over all wavelengths in the range of 360–460 nm using the angularly resolved spectra of TH waves (see below). At a low pump energy of 240 μJ, the TH beam is predominantly composed of an axial component, surrounded by a weak ring component as shown in Figs. 2(a) and 2(d). Increasing the pump energy to 360 μJ will greatly enhance the ring emission, as can be seen in Figs. 2(b) and 2(e); however, the axial emission still shows an intensity higher than that of the ring emission. When the pump energy is further increased to 478 μJ, a ring-shaped TH beam is formed as shown in Fig. 2(c). The disappearance of the axial component in Fig. 2(c) can be explained by the blueshift of the axial emission of the TH beam [see Figs. 3(c) and 3(d)], because our CCD camera is insensitive to the UV spectral range. In fact, the intensity of the axial emission in Fig. 2(e) is comparable to that of the ring emission, as indicated by Fig. 2(f).

The transformation of the TH beam shape following the increasing pump energy implies that one or more nonlinear optical effects are playing important roles in the THG process during the filamentation. To get more insight into the underlying physics, we record the angularly resolved spectra of TH waves generated at different pump energies, as shown

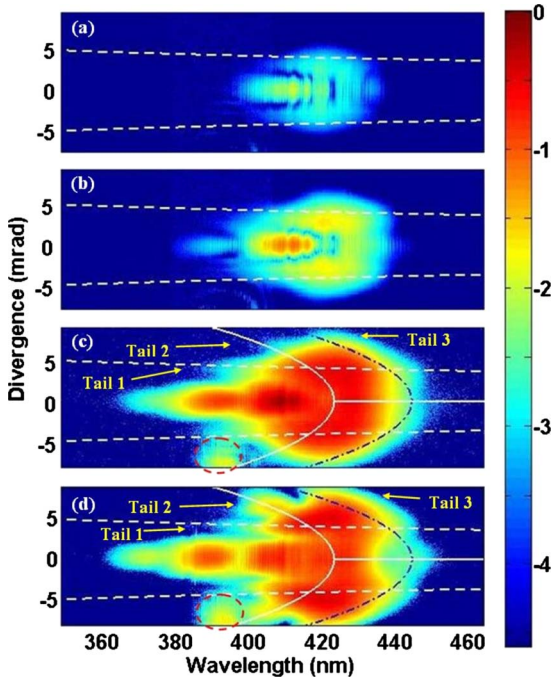

FIG. 3. (Color online) Normalized angular resolved spectrum of TH in air with FW pulse energy at (a) 135 μJ, (b) 240 μJ, (c) 410 μJ, and (d) 481 μJ (in logarithmic scale and normalized by the maximum intensity of TH). The signal indicated by the dashed ring is the remaining SH of the 800 nm pump wave from the OPA.

in Fig. 3. The angular spectra recorded at 135 μJ and 240 μJ, as shown in Figs. 3(a) and 3(b), are clearly composed of a ring and an axial component. After a further increase of the pump energy to 410 μJ and 481 μJ, symmetrical X-shaped tails start to appear in the angular spectra, as indicated in Figs. 3(c) and 3(d) by solid and dash-dotted lines. In general, the hyperbolic-structured tails are signatures of X waves. Spectral interference was also observed in the axial TH, which might be caused by pulse splitting [29] or pulse steepening [30].

We now show that in the formation of the tails during IR ultrashort pulse filamentation, two mechanisms can play important roles. The first mechanism is the phase matching between the generated TH and the fundamental wave (FW), which requires $k_z(\omega)=3k(\omega/3)$. Here ω is the frequency of the TH wave, and $k(\omega)$ and $k(\omega/3)$ are the wave vectors of TH and fundamental waves, respectively. Note that we have assumed that the laser beam propagates along the z direction. The phase-matching angle can therefore be expressed as [24]

$$\theta(\omega)=\tan^{-1}\left\{\frac{\sqrt{2k_z(\omega)[k_z(\omega)-3k_z(\omega/3)]}}{k_z(\omega)}\right\}. \quad (1)$$

In order to fulfill the momentum conservation law, a three-wave mixing picture is employed in which the angularly resolved TH spectrum can be viewed as a result of scattering of the incident fundamental carrier wave off the "scattering potential" due to the nonlinear response of the medium [24]. The dashed curves in Figs. 3(a)–3(d) mark the locus of phase matching between the TH and FW calculated using Eq. (1).

It is clearly shown in Figs. 3(c) and 3(d) that the tail corresponding to the lower divergence angle (tail 1) almost perfectly overlaps the dashed curve. This provides strong evidence that phase-matching between the TH and FW is the dominant mechanism for formation of the tail.

Further increase of the pump pulse leads to the formation of two X-shaped tails (tails 2 and 3), as shown in Figs. 3(c) and 3(d). These two tails can be fitted with the equations below [31].

$$k_z = (k_0 - \beta) + (k_0' - \alpha)\Omega = (k_0 - \beta) + \Omega/V_g, \tag{2}$$

$$k_\perp = \sqrt{k^2 - k_z^2}, \tag{3}$$

$$\theta(\omega) = \tan^{-1}(k_\perp/k_z), \tag{4}$$

where $k=\omega n(\omega)/c$, $k_0=k(\omega_0)$, k_0' is the first derivative of $k(\omega)$ evaluated at ω_0, $\Omega=\omega-\omega_0$, and β and α are corrections to the phase and group velocity, respectively. The tail 2 in either Fig. 3(c) or Fig. 3(d) is fitted by setting a central wavelength at 423 nm, $\beta=0$ and $V_g=(k_0'-\alpha)^{-1}\approx 2.9985\times 10^8$ m/s in Eqs. (2)–(4) (solid curves), whereas the tail 3 in either Fig. 3(c) or Fig. 3(d) is fitted by shifting the central wavelength to 444 nm in Eqs. (2)–(4), but maintaining $\beta=0$ and $V_g=(k_0'-\alpha)^{-1}\approx 2.9985\times 10^8$ m/s (dash-dotted curves). It can clearly be seen in Fig. 3 that the calculated curves and the X-shaped tails in the angular spectra match reasonably well. Based on these findings, we speculate that a pair of TH X waves with slightly different central wavelengths have been formed after the IR ultrashort pulse filamentation process owing to the splitting of the fundamental driving pulse, because after pulse splitting the leading pulse could be redshifted. One may have noticed that these two X-shaped tails (tails 2 and 3) only appear at a pump energy higher than that needed for the formation of the tail 1. This could be caused by the larger cone angles of the TH X waves. In this case, higher intensity of the pump pulse will induce larger modulation of the polarization of the medium, which in turn results in a larger divergence angle of the scattered TH wave. Only when the divergence angle of the scattered TH wave reaches the cone angles of the tails 2 and 3 can the formation of the TH X waves be initiated with a sufficiently strong seed. This also partially explains why it is difficult to obtain X-shaped TH waves with 800 nm pump pulses, as in that case the required cone angles of TH X waves could be significantly larger due to the fact that dispersion in the visible-ultraviolet range is higher than that in the visible-infrared range.

Figure 4(a) shows the conversion efficiencies of total TH, axial component of TH, and ring component of TH as functions of the pump energy. For comparison, the ratios of the axial and ring components to the total TH as functions of the pump energy are shown in Fig. 4(b). One can clearly see in Fig. 4(a) that at a pump energy between 30 μJ and 200 μJ, the conversion efficiencies of both the ring and axial components increase with the increasing pump energy at a relatively low conversion ratio, whereas Fig. 4(b) further reveals a faster growth of the ring component than that of the axial one. When the pump energy is raised to 200 μJ and 400 μJ,

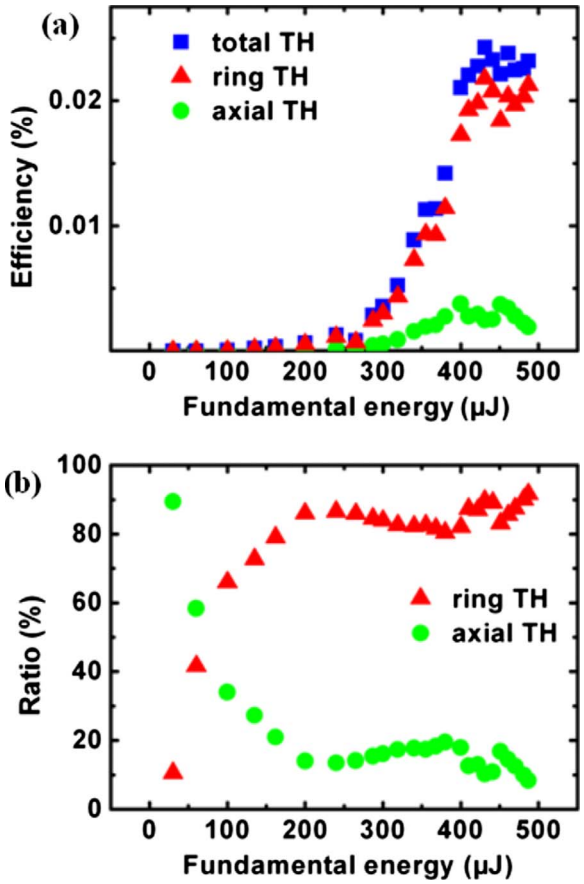

FIG. 4. (Color online) (a) Conversion efficiency of the TH generated in atmospheric air as a function of pump energy, and (b) ratio of the TH central part and TH rings over the total TH energy as a function of pump energy.

the ratio of the ring and axial components to the total TH appears constant, indicating that filamentation might have occurred at the pump energy of ~200 μJ [32,33]. Further raising the pump energy above ~400 μJ, it is clearly shown in Fig. 4(b) that the ratio of the ring component to total TH begins to increase again; on the contrary, the ratio of the axial component to total TH begins to decrease [32,33]. It has been shown in Fig. 3 that the X-shaped TH wave can only be observed in the angularly resolved spectrum at a pump energy approaching ~400 μJ, therefore, the sudden increase of the ratio between the ring component to total TH could be attributed to the formation of the X-shaped TH wave, which might be a result of the group velocity matching between the TH and FW. Further experimental investigation is desirable to determine both the group velocities of the FW and TH simultaneously in order to justify this conjecture.

IV. CONCLUSIONS

To summarize, we systematically investigate the evolution of an angular spectrum of the TH wave generated by IR ultrashort pulse filamentation in air. The use of a mid-IR

pump beam allows us to shift the central wavelength of the TH beam to a visible range, a unique property unattainable with the popularly used Ti:sapphire laser with a wavelength centered at ~800 nm. The visible TH beam can easily be detected without losing any spectral information. We speculate that there exist two physical mechanisms governing the evolution of an angular spectrum of the TH wave, implying different origins of a conical ring and X wave. Further effort will be made on the establishment of a link between the angular spectra of fundamental and TH waves. In that way, the TH wave in the visible range could be used as a probe beam for determining the spatial-spectral property of the IR fundamental wave, making it unnecessary to use an expensive IR detector.

ACKNOWLEDGMENTS

This work was supported by the National Basic Research Program of China (Grant No. 2006CB806000), Shanghai Commission of Science and Technology (Grant No. 07JC14055), and National Natural Science Foundation of China (Grant No. 10523003). Y.C. acknowledges the support of 100 Talents Program of the Chinese Academy of Sciences. S.L.C. acknowledges the support of the Canada Research Chairs program.

[1] P. Rairoux *et al.*, Appl. Phys. B: Lasers Opt. **71**, 573 (2000).
[2] J. Kasparian *et al.*, Science **301**, 61 (2003).
[3] J. F. Gravel, Q. Luo, D. Boudreau, X. P. Tang, and S. L. Chin, Anal. Chem. **76**, 4799 (2004).
[4] Xin Miao Zhao, J. C. Diels, C. Y. Wang, and J. M. Elizondo, IEEE J. Quantum Electron. **31**, 599 (1995).
[5] H. Pepin *et al.*, Phys. Plasmas **8**, 2532 (2001).
[6] M. Rodriguez *et al.*, Opt. Lett. **27**, 772 (2002).
[7] C. P. Hauri, W. Kornelis, F. W. Helbing, A. Heinrich, A. Couairon, A. Mysyrowicz, J. Biegert, and U. Keller, Appl. Phys. B: Lasers Opt. **79**, 673 (2004).
[8] X. W. Chen, X. F. Li, J. Liu, P. F. Wei, X. C. Ge, R. X. Li, and Z. Z. Xu, Opt. Lett. **32**, 2402 (2007).
[9] N. Akozbek *et al.*, New J. Phys. **8**, 177 (2006).
[10] C. Wang, Y. X. Fu, Z. H. Zhou, Y. Cheng, and Z. Z. Xu, Appl. Phys. Lett. **90**, 181119 (2007).
[11] S. L. Chin *et al.*, Can. J. Phys. **83**, 863 (2005).
[12] L. Berge, S. Skupin, R. Nuter, J. Kasparian, and J. P. Wolf, Rep. Prog. Phys. **70**, 1633 (2007).
[13] A. Couairon and A. Mysyrowicz, Phys. Rep. **441**, 47 (2007).
[14] S. Backus, J. Peatross, Z. Zeek, A. Rundquist, G. Taft, M. M. Murnane, and H. C. Kapteyn, Opt. Lett. **21**, 665 (1996).
[15] A. B. Fedotov, N. I. Koroteev, M. M. T. Loy, X. Xiao, and A. M. Zheltikov, Opt. Commun. **133**, 587 (1997).
[16] J. Peatross, S. Backus, J. Zhou, M. M. Murnane, and H. C. Kapteyn, J. Opt. Soc. Am. B **15**, 186 (1998).
[17] N. Aközbek, A. Iwasaki, A. Becker, M. Scalora, S. L. Chin, and C. M. Bowden, Phys. Rev. Lett. **89**, 143901 (2002).
[18] C. W. Siders, N. C. Turner, M. C. Downer, A. Babine, A. Stepanov, and A. M. Sergeev, J. Opt. Soc. Am. B **13**, 330 (1996).
[19] H. R. Lange, A. Chiron, J. F. Ripoche, A. Mysyrowicz, P. Breger, and P. Agostini, Phys. Rev. Lett. **81**, 1611 (1998).
[20] N. Kortsalioudakis *et al.*, Appl. Phys. B: Lasers Opt. **80**, 211 (2005).
[21] G. Marcus, A. Zigler, and Z. Henis, J. Opt. Soc. Am. B **16**, 792 (1999).
[22] G. L. Mao, Y. H. Wu, and K. D. Singer, Opt. Express **15**, 4857 (2007).
[23] M. L. Naudeau, R. J. Law, T. S. Luk, T. R. Nelson, S. M. Cameron, and J. V. Rudd, Opt. Express **14**, 6194 (2006).
[24] M. Kolesik, E. M. Wright, A. Becker, and J. V. Moloney, Appl. Phys. B: Lasers Opt. **85**, 531 (2006).
[25] M. Kolesik, E. M. Wright, and J. V. Moloney, Opt. Lett. **32**, 2816 (2007).
[26] H. Xu, H. Xiong, R. X. Li, Y. Cheng, Z. Z. Xu, and S. L. Chin, Appl. Phys. Lett. **92**, 011111 (2008).
[27] D. Faccio, P. Di Trapani, S. Minardi, A. Bramati, F. Bragheri, C. Liberale, V. Degiorgio, A. Dubietis, and A. Matijosius, J. Opt. Soc. Am. B **22**, 862 (2005).
[28] D. Faccio, M. A. Porras, A. Dubietis, F. Bragheri, A. Couairon, and P. Di Trapani, Phys. Rev. Lett. **96**, 193901 (2006).
[29] A. Couairon, E. Gaižauskas, D. Faccio, A. Dubietis, and P. Di Trapani, Phys. Rev. E **73**, 016608 (2006).
[30] O. G. Kosareva (private communication).
[31] D. Faccio *et al.*, Opt. Express **15**, 13077 (2007).
[32] F. Theberge, N. Akozbek, W. Liu, J. F. Gravel, and S. L. Chin, Opt. Commun. **245**, 399 (2005).
[33] F. Theberge, N. Akozbek, W. Liu, J. Filion, and S. L. Chin, Opt. Commun. **276**, 298 (2007).